Contents lists available at SciVerse ScienceDirect

Computational Materials Science

A new approach for determination of material constants of internal state variable based plasticity models and their uncertainty quantification

S. Salehghaffari, M. Rais-Rohani *, E.B. Marin, D.J. Bammann

Mississippi State University, MS 39762, USA

ARTICLE INFO

ABSTRACT

Physically-based plasticity models such as the BCJ model include internal state variables that represent the current state of the material and allow capturing strain rate and temperature history effects as well as the coupling of rate- and temperature-dependence with material hardening. However, the inclusion of internal state variables increases significantly the number of unknown material constants that need to be found through fitting of the model to experimental stress–strain data at different strain rates and temperatures. This makes the fitting process extremely challenging and increases the uncertainty in the material constants. The paper presents a physics-guided numerical fitting approach that reduces the associated difficulties and uncertainties involved in determining the material constants of the BCJ plasticity model. The approach uses experimental data from monotonic and reverse loading stress–strain curves at different temperatures and strain rates to determine the 18 material constants of the model. An evidential uncertainty quantification approach is used to determine uncertainties rooted in experimental data, selection of stress–strain curves at different loading conditions, variability of material properties, numerical aspects of the fitting method and mathematical formulations of the BCJ model. The represented uncertainty of the BCJ material constants based on mathematical tools of evidence theory is propagated through Taylor impact simulations of a 7075-T651 aluminum alloy cylinder. Uncertainty quantification results verify the presented numerical fitting approach for the BCJ model and its potential applicability to other similar material models.

1. Introduction

Several plasticity and coupled plasticity-damage models have been developed and used to simulate the large inelastic deformation of solids and structures subjected to different loading rates and temperatures. Simple empirical models, such as the power law, Johnson–Cook [1,2] and modified Johnson–Cook [3] models, as well as physically-motivated models, such as Zerilli–Armstrong [2,4] and Usui [5] models are equation-of-state models that represent the flow stress as a unique function of total strain, strain rate, and temperature, independent of the loading path. More accurate representation of material behavior have been developed using physically-based plasticity models that include history dependent internal state variables (ISVs) representing the current state of the material and capturing strain rate and temperature history effects as well as the coupling of rate- and temperature-dependence with material hardening. Among these models are the Bammann–Chiesa–Johnson (BCJ) model [6–8], the BCJ-damage model [9], and the Evolving Microstructural Model of Inelasticity (EMMI) [10].

All plasticity models cited above include a number of material constants that capture different aspects of the material properties, and as such, take different values depending on the material considered. The calculation of these unknown constants for any specific material requires fitting the plasticity model to experimental stress–strain curves obtained under various loading paths (compression, tension and torsion) and at different strain rates and temperatures. However, for a given material constant, the fitting process may yield different values as a result of the existing uncertainty in the experimental procedure, different selection of stress–strain curves covering a range of strains, temperatures and rates as well as existing uncertainty in the numerical aspects of the fitting process such as selection of different starting point and numerical method. Such existing uncertainty in material constants can propagate into a simulation response and jeopardize the accuracy of the simulation results. In a recent study at Los Alamos National Lab., Gray et al. [11] examined both Johnson–Cook [1,2] and Zerilli–Armstrong [2,4] constitutive models and recognized that fitting these models using different sets of data can result in quite different values of the material constants. This issue is more critical for ISV plasticity models, such as the BCJ model [6–9], as the number

* Corresponding author. Address: Aerospace Engineering Department and Center for Advanced Vehicular Systems, MS, USA. Tel.: +1 662 325 7294; fax: +1 662 325 7730.
   E-mail address: Masoud@ae.msstate.edu (M. Rais-Rohani).

of unknown material constants can increase considerably. In fact, the task of fitting the large number of material constants in advanced plasticity models is more difficult and burdened by greater uncertainty.

Because of their non-physical nature, traditional fitting approaches [12], which rely heavily on the numerical aspects of fitting, are incapable of dealing with the existing uncertainty when computing the material constants for advanced plasticity models. Such difficulties are addressed in this paper by introducing a physics-guided numerical fitting approach that can help to reduce the existing uncertainty through physical interpretation of the fitting process. The determination of the material constants for the BCJ plasticity model is considered for this purpose. At first, the approach uses experimental data on forward-to-reverse yield of 7075-T651 aluminum alloy to determine those material constants representing strain hardening effects with consideration of Bauschinger effects. Then, four stress–strain curves at high and low temperatures and rates are used to determine material constants of flow rule in BCJ plasticity model. An evidence based uncertainty quantification approach is also employed to model uncertainty of material constants.

This study is organized into two parts. The first part presents the constitutive equations of the BCJ plasticity model along with the proposed fitting approach for computing the corresponding material constants. The second part deals with different aspects of uncertainty quantification (representation, propagation and measurement) as applied to the BCJ model using the framework of evidence theory.

2. Constitutive equations of BCJ plasticity model

The BCJ plasticity model, developed by Bammann et al. [6–8], is a dislocation-based ISV model that describes the rate- and temperature-dependent finite deformation behavior of ductile metals. The complete version of the model is envisioned to have a number of ISVs that should represent such material features as dislocation hardening, void-induced damage, plastic anisotropy, recrystallization and grain growth, as well as deformation-induced phase transformations. The particular version of the model used in this work mainly accounts for the plasticity aspects of the material response, i.e., the kinetics of plastic flow and dislocation hardening. In essence, this particular version of the model (a) introduces a dynamic yield surface whose evolution is governed by temperature, strain rate and stress state; and (b) contains two plastic state variables representing isotropic and kinematic hardening which model, respectively, the size and location of the dynamic yield surface. The evolution equations of these variables assume that the material hardening processes such as storage of dislocations (isotropic hardening) and formation of cells and cell boundaries (kinematic hardening) are balanced by recovery processes such as dislocation cross slip and dislocation climb.

The basic formulation of the plasticity and temperature aspects of the model relies on an extended description of the large deformation kinematics using the multiplicative decomposition of the deformation gradient into thermal, plastic and elastic components. This kinematics coupled with a thermodynamic approach with ISVs, as proposed by Coleman and Gurtin [13], gives the formulation of BCJ a strong mathematical basis that relies upon very well known principles of continuum mechanics. The 3-D model equations defined by Eqs. (1)–(5) below describes the kinematics, the elastic law, and the plasticity (flow rule and hardening laws), and are valid for small elastic strains (typical in metals).

$$\underline{\sigma}^{\circ} = \underline{\dot{\sigma}} - \underline{W}^e\underline{\sigma} + \underline{\sigma}\underline{W}^e = \lambda tr(\underline{D}^e)\underline{I} + 2\mu\underline{D}^e \tag{1}$$

$$\underline{D}^e = \underline{D} - \underline{D}^{in} - \underline{D}^{th}, \quad \underline{W}^e = \underline{W} - \underline{W}^P \tag{2}$$

Table 1
Relationship between parameter functions and material constants of the BCJ plasticity model.

$V(T) = C_1 \exp(-C_2/T)$	$r_s(T) = C_{11} \exp(-C_{12}/T)$
$Y(T) = C_3 \exp(C_4/T)$	$R_d(T) = C_{13} \exp(-C_{14}/T)$
$f(T) = C_5 \exp(-C_6/T)$	$H(T) = C_{15} \exp(C_{16}/T)$
$r_d(T) = C_7 \exp(-C_8/T)$	$R_s(T) = C_{17} \exp(-C_{18}/T)$
$h(T) = C_9 \exp(C_{10}/T)$	

$$\underline{D}^{in} = \sqrt{\frac{2}{3}}\dot{\varepsilon}^p\underline{N}, \quad \dot{\varepsilon}^p = f(T)\sinh\left[\frac{\bar{\sigma} - (R + Y(T))}{V(T)}\right] \tag{3}$$

$$\underline{\alpha}^o = \underline{\dot{\alpha}} - \underline{W}^e\underline{\alpha} + \underline{\alpha}\underline{W}^e = h(T)\underline{D}^{in} - [r_d(T)\dot{\varepsilon}^p + r_s(T)]\sqrt{\frac{2}{3}}\|\underline{\alpha}\|\underline{\alpha} \tag{4}$$

$$\dot{R} = H(T)\dot{\varepsilon}^p - [R_d(T)\dot{\varepsilon}^p + R_s(T)]R^2 \tag{5}$$

where $\bar{\sigma} = \sqrt{\frac{3}{2}}\|\underline{\xi}\|$, $\underline{N} = \frac{\underline{\xi}}{\|\underline{\xi}\|}$, $\underline{\xi} = \underline{\sigma}' - \frac{2}{3}\underline{\alpha}$, $\underline{\sigma}' = \underline{\sigma} - \sigma_m\underline{I}$.

with $\sigma_m = 1/3\sigma_{kk}$. In Eq. (1), $\underline{\sigma}^\circ$ is an objective stress rate, λ and μ are the Lamés constants, $\underline{\sigma}$ is the Cauchy stress, $\underline{W}^e$ is the elastic spin, $\underline{I}$ is the identity tensor, and $tr(\bullet)$ is the trace operator. Decomposing the skew symmetric and symmetric parts of the velocity gradient into elastic and plastic parts, one derives Eq. (2) that is written for the elastic stretching $\underline{D}^e$ and the elastic spin $\underline{W}^e$. In this equation, $\underline{D}^{in}$ is the deviatoric inelastic strain rate, $\underline{D}^{th}$ is the stretching rate due to the thermal expansion, and $\underline{W}^P$ is the plastic spin assumed to be zero here. Here, $\underline{D}$ and $\underline{W}$ denote the total deformation and spin which are defined by the boundary conditions. As shown by Eq. (3), the deviatoric inelastic flow rule $\underline{D}^{in}$ that encompasses the regimes of creep and plasticity is a function of the kinematic and isotropic ISVs $\underline{\alpha}$ and R, respectively, and the functions $f(T)$, $V(T)$ and $Y(T)$ which have an Arrhenius-type temperature dependence. The evolution equations of $\underline{\alpha}$ and R are presented in a hardening-minus-recovery format by Eqs. (4) and (5) in which $h(T)$ and $H(T)$ are the hardening moduli, $r_d(T)$ and $R_d(T)$ are the functions describing dynamic recovery, $r_s(T)$ and $R_s(T)$ are the functions representing static recovery, and $\|(\bullet)\|$ is the norm operator. The temperature dependence of these material functions are summarized in Table 1, where the C_i, $i = 1, 18$ are material constants or parameters. Note that these parameters include sources of uncertainty reflecting indirectly the variability and incertitude in the material microstructure. The BCJ plasticity model is implemented in LSDYNA as MAT_051 with the material constants in Table 1 defined as input parameters.

3. BCJ equations for the case of uniaxial stress

The unknown material constants of the BCJ model shown in Table 1 are determined by comparing model predictions to experimental data from specimens under uniform stress states (e.g. uniaxial stress–strain curves) at constant temperatures and strain rates. For the case of uniaxial stress (tension or compression) under isothermal conditions, the BCJ model equations reduce to

$$\dot{\sigma} = E(\dot{\varepsilon} - \dot{\varepsilon}^p) \tag{6}$$

$$\dot{\varepsilon}^p = f(T)\sinh\left[\frac{|\sigma - \alpha| - R - Y(T)}{V(T)}\right]\text{sign}(\sigma - \alpha) \tag{7}$$

$$\dot{\alpha} = h(T)\dot{\varepsilon}^p - [r_d(T)|\dot{\varepsilon}^p| + r_s(T)]\alpha^2\text{sign}(\alpha) \tag{8}$$

$$\dot{R} = H(T)|\dot{\varepsilon}^p| - [R_d(T)|\dot{\varepsilon}^p| + R_s(T)]R^2 \tag{9}$$

where σ is the only non-vanishing component of the Cauchy stress tensor; α, $\dot{\varepsilon}$, and $\dot{\varepsilon}_p$ are the normal components along the principal axis of tensors $\underline{\alpha}$, $\underline{D}$, and $\underline{D}^{in}$, respectively.

Here, we assume that shortly after the yield point, the plastic strain rate $\dot{\varepsilon}_p$ can be reasonably approximated by the total strain rate $\dot{\varepsilon}$, i.e., $\dot{\varepsilon} \approx \dot{\varepsilon}_p$ (viscoplasticity). Also, for each experimental stress–strain curve, the temperature T and strain rate $\dot{\varepsilon}$ are constant; hence, the variables are mainly functions of strain ε. Considering this fact and employing the chain rule of differentiation, one can show that for each experimental strain–stress curve, the time derivatives of α and R can be expressed as: $\dot{\alpha} = \frac{d\alpha}{dt} = \frac{\dot{\varepsilon} d\alpha}{d\varepsilon}, \dot{R} = \frac{dR}{dt} = \frac{\dot{\varepsilon} dR}{d\varepsilon}$. Considering these assumptions, Eqs. (7)–(9) can then be written as

$$\dot{\varepsilon} = f \sinh \left[\frac{|\sigma - \alpha| - R - Y}{V} \right] \text{sign}(\sigma - \alpha) \tag{10}$$

$$\dot{\varepsilon}\frac{d\alpha}{d\varepsilon} = h\dot{\varepsilon} - [r_d|\dot{\varepsilon}| + r_s]\alpha^2 \text{sign}(\alpha) \tag{11}$$

$$\dot{\varepsilon}\frac{dR}{d\varepsilon} = H|\dot{\varepsilon}| - [R_d|\dot{\varepsilon}| + R_s]R^2 \tag{12}$$

The integration of Eqs. (11) and (12), with the initial values of α and R set to zero, yields

$$\alpha = \sqrt{\frac{h\dot{\varepsilon}}{(r_d\dot{\varepsilon} + r_s)}} \tanh \left(\frac{\varepsilon\sqrt{h\dot{\varepsilon}(r_d\dot{\varepsilon} + r_s)}}{\dot{\varepsilon}} \right) \tag{13}$$

$$R = \sqrt{\frac{H\dot{\varepsilon}}{(R_d\dot{\varepsilon} + R_s)}} \tanh \left(\frac{\varepsilon\sqrt{H\dot{\varepsilon}(R_d\dot{\varepsilon} + R_s)}}{\dot{\varepsilon}} \right) \tag{14}$$

By inverting the flow rule in Eq. (10) and substituting Eqs. (13) and (14), one obtains

$$\sigma = \sqrt{\frac{h\dot{\varepsilon}}{(r_d\dot{\varepsilon} + r_s)}} \tanh \left(\frac{\varepsilon\sqrt{h\dot{\varepsilon}(r_d\dot{\varepsilon} + r_s)}}{\dot{\varepsilon}} \right) + \sqrt{\frac{H\dot{\varepsilon}}{(R_d\dot{\varepsilon} + R_s)}}$$
$$\times \tanh \left(\frac{\varepsilon\sqrt{H\dot{\varepsilon}(R_d\dot{\varepsilon} + R_s)}}{\dot{\varepsilon}} \right) + Y + V\sinh^{-1}\left(\frac{\dot{\varepsilon}}{f}\right) \tag{15}$$

Eq. (15) describes the stress as a function of the ISVs, strain rate and temperature.

4. The new physics-guided fitting approach

The ability of the BCJ plasticity model to predict the mechanical behavior of metals under different temperatures and strain rates is strongly dependent upon the correct determination of its eighteen material constants. Recently, Guo et al. [12] determined the BCJ material constants for Ti–6Al–4 V titanium, AISI 52100 steel, and 6061-T6 aluminum alloy through nonlinear least-squares fitting of the BCJ model to experimental stress–strain data of the respective materials. One observation they made was that the arbitrary choice of starting values for the constants in the nonlinear fitting procedure does not guarantee the best fit. Considering that no physical bounds have been established for the eighteen material constants of BCJ plasticity model, the task of finding the best fit can be very tedious and present a source of uncertainty. To address this challenging task, Guo et al. [12] began by fitting approximately three constants at a time while holding the others fixed, and monitored the fitting improvement by checking the maximum and average residual (fitting errors) as a reference to tune the constants in each attempt until a satisfactory fit was obtained. However, that fitting approach is tedious, nonphysical, and relies heavily on the numerical aspects of fitting. In fact, all constants can be fitted simultaneously with stress–strain data at different temperatures and strain rates with no physical interpretation of the fitting

procedure. That approach also requires a large number of stress–strain curves, which may not be practical when faced with scarcity of data for a particular material. In this section, we introduce a physics-guided numerical fitting approach to address the difficulties in determining the constants of BCJ plasticity model.

For stress–strain curves at a constant temperature, the parameter functions of the BCJ model in Table 1 will have a fixed value for temperature. The proposed fitting approach suggests fitting of the parameter functions with two separate sets of stress–strain curves at low and high temperatures. While reducing the unknown constants from eighteen to nine, this procedure requires the duplication of the fitting process for sets of stress–strain curves at two different temperatures. Suppose that for an arbitrary parameter function $Y(T)$ of the same general form as those in Table 1, i.e., $Y(T) = C_1\exp(C_2/T)$, two values (say Y_1 and Y_2) are known through fitting the model with two different sets of stress–strain curves of various strain rates at low temperature T_1 and high temperature T_2. Then, constants C_1 and C_2 can be easily determined using the following equations:

$$C_2 = \frac{T_1 T_2}{T_2 - T_1} ln\left(\frac{Y_1}{Y_2}\right) \tag{16a}$$

$$C_1 = Y_1 \exp\left(\frac{-T_2}{(T_2 - T_1)} ln\left(\frac{Y_1}{Y_2}\right)\right) \tag{16b}$$

Hence, using the above formulations, material constants that represent the material behavior at different temperatures and strain rates can be determined. This decreases uncertainty in the traditional fitting approach by considering the material behavior at different temperatures and reducing the number of constants that need to be fitted simultaneously.

In addition, as will be explained, the proposed fitting method suggests fitting the unknown constants of the evolution equations for the hardening variables (Eqs. (11) and (12)) and the equation for the flow stress (inverse of Eq. (10)) separately in different stages while keeping the physical link and flow of information among them. This reduces the fitting of nine parameters to three at a time in three stages, easing the process of fitting. Details of the physics-guided numerical fitting approach are provided below.

4.1. Evaluation of hardening parameters

Loading and unloading experiments on many ductile materials have shown that the flow stress in reverse direction softens sooner than that of forward direction, as shown in Fig. 1, resulting in the reduction of reverse flow, a phenomenon known as Baushinger effect [14]. This behavior is mainly because the mechanical response of metals in plastic deformation is affected by deformation history in addition to the current stress state. The physics-guided fitting approach considers such effects in computing the hardening constants through experimental evaluation of the ISVs α and R using
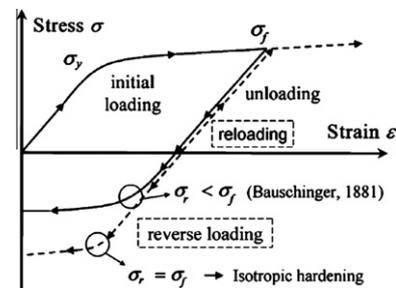

Fig. 1. Quantification of σ_f, σ_r, σ_y from experimental stress strain curve [14].

forward-to-reverse yield data of materials at different temperatures and strain rates.

The experimental values of ISVs α and R can be found through definition of the von-Misses yield surface for both forward and reverse loading as given by

$$|\sigma_f - \alpha| - R - \sigma_y = 0 \qquad (17)$$

$$|\sigma_r - \alpha| - R - \sigma_y = 0 \qquad (18)$$

where σ_f, σ_r, σ_y are the forward yield, reverse yield, and initial yield stress, respectively (see Fig. 1). As $\sigma_f - \alpha > 0$ and $\sigma_r - \alpha < 0$ ($\sigma_r < 0$), one can derive from the Eqs. (17) and (18) the expressions for α and R as

$$\alpha = \frac{\sigma_f + \sigma_r}{2} \qquad (19)$$

$$R = \frac{\sigma_f - \sigma_r}{2} - \sigma_y \qquad (20)$$

The constants of the hardening evolution equations are derived as follows:

- *Step 1*: Collect forward-to-reverse yield data of material at different strains and strain rates at a low temperature T1.
- *Step 2*: Quantify experimental values of hardening parameters α and R using Eqs. (19) and (20) and the collected data in Step 1.
- *Step 3*: Fit Eqs. (13) and (14) individually using the α and R values found in Step 2 and the nonlinear least-squares fitting approach to determine values of the hardening functions h, rs, rd, H, Rs and Rd for T1.
- *Step 4*: Repeat Steps 1–3 for a high temperature T2; and
- *Step 5*: Use Eqs. (16a) and (16b) along with the derived parameters of the evolution equations at temperatures T1 and T2 to solve for the corresponding material constants (C7–C18).

4.2. Evaluation of flow parameters

After computing the 12 hardening constants, the additional six constants for the flow rule are determined using four stress–strain curves under monotonic loading: two (low and high strain rates) at a low temperature and the other two (also low and high strain rates) at a high temperature. Note that the parameters of the hardening evolution equations in Eq. (15) are known from the fitting procedure above. Then, the unknown parameters to be fitted in Eq. (15) are Y, V and f. The step-by-step procedure to determine the constants of flow rule equation is as follows:

- *Step 1*: Fit Eq. (15) with two stress–strain curves of high and low strain rates simultaneously using a genetic algorithm-based multi-functional nonlinear least-squares fitting at low temperature T1 to determine unknown parameters of Y, V and f.
- *Step 2*: Repeat Step 1 for high temperature T2.
- *Step 3*: Use Eqs. (16a) and (16b) along with derived parameters of flow rule equation at temperatures T1 and T2 to solve for the corresponding material constants (C1–C6).

4.3. Determination of BCJ constants for AL 7075-T651

As an illustrative example of the presented fitting approach, the material constants of 7075-T651 aluminum alloy are determined using the experimental data provided in [14–17]. Forward-to-reverse yield of this alloy at different strains, temperatures, and strain rates as shown by Table 2 are used to estimate the experimental values of α and R. Fitting the hardening evolution equations of the BCJ model using the data in Table 2 yields the corresponding material constants C_7–C_{18} as shown in Table 3. The material constants C_1–C_6 of the flow rule are computed using

Table 2
Evaluation of state variables α and R at different strains, temperatures and strain rates.

ε	σ_y (MPa)	σ_f (MPa)	σ_r (MPa)	α (MPa)	R (MPa)
$T = 297\ K,\ \dot{\varepsilon} = 0.1$					
0.01	454	521	−439	41	26
0.03	454	549	−390	79.5	15.5
0.05	454	583	−363	110	19
$T = 673\ K,\ \dot{\varepsilon} = 0.01$					
0.04	60.3	65.3	−60.3	2.5	2.5
0.31	60.3	63.3	−61.4	0.95	2.05
0.55	60.3	61.8	−59.2	1.3	0.2

four stress–strain curves at different strain rates and temperatures (see Fig. 2). Fig. 2 compares the generated stress–strain curves by the BCJ model using the derived constants in Table 3 with experimental data that are used in the fitting process. As expected, the generated curves and those from the experiments match very well. As an additional check, the computed constants in Table 3 are used to predict the experimental stress–strain curves at other temperatures and strain rates. The predicted and experimental response curves are shown in Fig. 3. As observed, there is a fairly good agreement between experimental and predicted curves. This verifies the accuracy of the BCJ material constants using the presented fitting approach.

5. Uncertainty in BCJ plasticity model

As shown in Table 4, depending on the selected sets of stress–strain curves at different strain rates and temperatures, the proposed fitting approach produces different values for some of the BCJ material constants for 7075-T651 aluminum alloy. Note that for all sets of material constants in Table 4, experimental data provided by Table 2 is used for determination of hardening constants (i.e., C_7–C_{18}) that take the same values as those in Table 3. However, different sets of stress–strain curves as shown in Table 5 are used to fit the constants of BCJ flow equation, resulting in different sets of constants (i.e., C_1–C_6) in Table 4. This variability in the calculated material constants is mainly because of the uncertainty in the experimental procedure used to obtain the stress–strain curves, inherent variability in material properties, existing uncertainty in the numerical nonlinear least-squares fitting process, and incertitude or lack of knowledge in accurate modeling of the dynamic behavior of the material using the mathematical formulation of the BCJ plasticity model.

Considering the impact of BCJ material constants on simulation responses associated with a large deformation process (i.e., deep drawing, vehicle crash), it is necessary to quantify their uncertainty. Probability theory has been used in several investigations to model variability when sufficient information exists for defining each uncertain variable by a specific probability density function (PDF). Recently, modern approaches such as evidence theory [18,19], possibility theory [20], interval analysis [21] and imprecise probability theory [22] have been developed to quantify uncertainty when available knowledge of the problem is imprecise. Klir and Smith [23] give a detailed classification of these theories by levels of their generality and show that evidence theory is more general than the classical probability and possibility theories. Evidence theory offers a framework for modeling both incertitude (i.e., epistemic uncertainty) and random variability (i.e., aleatory uncertainty) through a more flexible representation of uncertainty. Evidence theory has attracted considerable interest in the fields of artificial intelligence, expert systems, and information fusion since the 1980s and is gaining increasing recognition in engineering applications [24–27].

Table 3
Calculated BCJ material constants for 7075-T651 aluminum alloy.

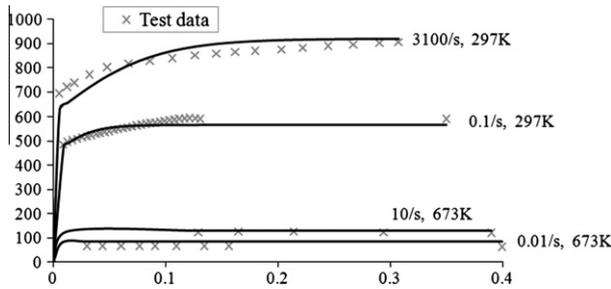| C_1 (MPa)	C_2 (K)	C_3 (MPa)	C_4 (K)	C_5 (1/s)	C_6 (K)	C_7 (MPa^{-1})	C_8 (K)	C_9 (MPa)
312.86	154.78	27.2	818.26	6914.10	233.39	9.00	1632.34	148.36
C_{10} (K)	C_{11} (s/MPa)	C_{12} (K)	C_{13} (MPa^{-1})	C_{14} (K)	C_{15} (MPa)	C_{16} (K)	C_{17} (s/MPa)	C_{18} (K)
942.28	100.67	2517.12	98.53	171.56	8950.63	279.18	7363.75	3316.82

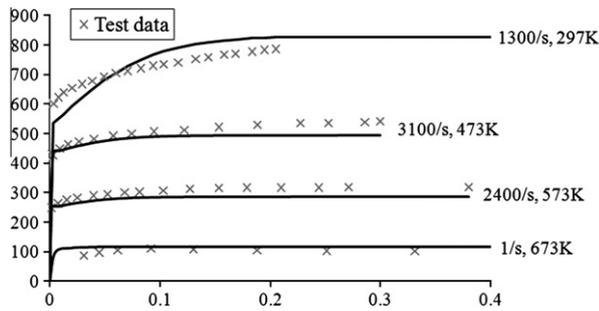**Fig. 2.** Comparison of the fitted curves and the corresponding experimental data.

Fig. 3. Comparison of the predicted curves and the corresponding experimental data.

Table 4
BCJ material constants for 7075-T651 aluminum alloy obtained using different sets of stress–strain curves.

No.	C_1 (MPa)	C_2 (K)	C_3 (MPa)	C_4 (K)	C_5 (s^{-1})	C_6 (K)
1	312.86	154.78	27.21	818.26	6914.10	233.39
2	406.37	182.63	22.67	890.84	7025.54	215.31
3	276.89	67.17	148.32	322.39	5829.39	155.30
4	304.34	167.24	31.88	670.20	7847.90	291.88
5	282.30	169.66	201.96	118.12	6697.24	249.90
6	368.68	247.98	178.41	250.38	8064.66	269.79
7	262.77	87.46	69.57	520.44	6229.10	186.33
8	339.31	205.59	137.33	317.34	6819.30	256.35
9	340.20	180.33	90.16	427.97	7532.25	293.39
10	333.46	167.69	35.31	736.58	7136.29	254.78
11	280.73	216.85	32.62	748.36	7398.12	258.42

Table 5
Testing conditions for the collected experimental data.

Curve No.	Ref. No.	Temperature (K)	Strain rate (s^{-1})	Curve No.	Ref. No.	Temperature (K)	Strain rate (s^{-1})
1	16	297	3100	9	15	673	10
2	16	297	2400	10	15	673	1
3	16	297	1300	11	15	673	0.1
4	14	297	0.1	12	15	673	0.01
5	15	573	10	13	15	723	10
6	15	573	1	14	15	723	1
7	15	573	0.1	15	15	723	0.1
8	15	573	0.01	16	15	723	0.01

Here, the available data for the BCJ material constants (see Table 4) is insufficient for assigning a particular PDF to each one, and our knowledge of the constants and modeling the dynamic material behavior of metals is imprecise. Hence, based on the nature of uncertainty in the BCJ plasticity model and the capabilities of evidence theory, we adopted this theory for uncertainty modeling of the BCJ plasticity model.

6. Evidential uncertainty reasoning of BCJ plasticity model

Before applying evidence theory for uncertainty modeling of BCJ plasticity model, a brief introduction is provided in this section. Evidence theory is also known as the Dempster–Shafer theory due to the fundamental work by Dempster [18] and Shafer [19]. For the sample space defined by the finite universal set $X = \{x_1, x_2, \ldots, x_n\}$, the frame of discernment represents all the possible propositions that can be expressed as the power set of X or $P(X) = 2^X = \{\varnothing, \{x_1\}, \{x_2\}, \ldots, \{x_n\}, \{x_1, x_2\}, \ldots, \{x_1, x_n\}, \ldots, \{x_1, x_2, \ldots, x_n\}\}$, where $\varnothing$ is the null set. The degree of belief in a particular proposition or element of $P(X)$ is quantified by the corresponding basic belief assignment (BBA) function m such that the three axioms (i.e., I. $m(\varnothing) = 0$, II. $m(A) \geqslant 0$ for $A \in P(X)$, and III. $\sum_{A \in P(X)} \{m(A) = 1\}$) are satisfied. The focal elements in $P(X)$ with $m \neq 0$ describe the so-called belief structure of x. In evidence theory, the total degree of belief in proposition B is described by belief and plausibility functions expressed as

$$Bel(B) = \sum_{A \subseteq B} m(A) \quad \text{for all} \quad B \subseteq X \tag{21}$$

$$Pl(B) = \sum_{A \cap B \neq \emptyset} m(A) \quad \text{for all} \quad B \subseteq X \tag{22}$$

where A represents different elements in $P(X)$. Epistemic uncertainty is measured as the gap between plausibility and belief with probability of proposition B bounded as $Bel(B) \leqslant P(B) \leqslant Pl(B)$. In contrast to probability theory, evidence theory suggests that the belief of a hypothesis and its complement plus the level of ignorance equals one or simply $Pl(B) + Bel(\neg B) = 1$.

Here, the evidential uncertainty reasoning approach successfully applied to uncertainty quantification (UQ) of Johnson–Cook plasticity model [28] is employed for quantification of uncertainty in BCJ plasticity model. The UQ framework is outlined by Fig. 4 and involves three necessary steps (uncertainty representation, propagation and measurement). As it can be realized, for uncertainty
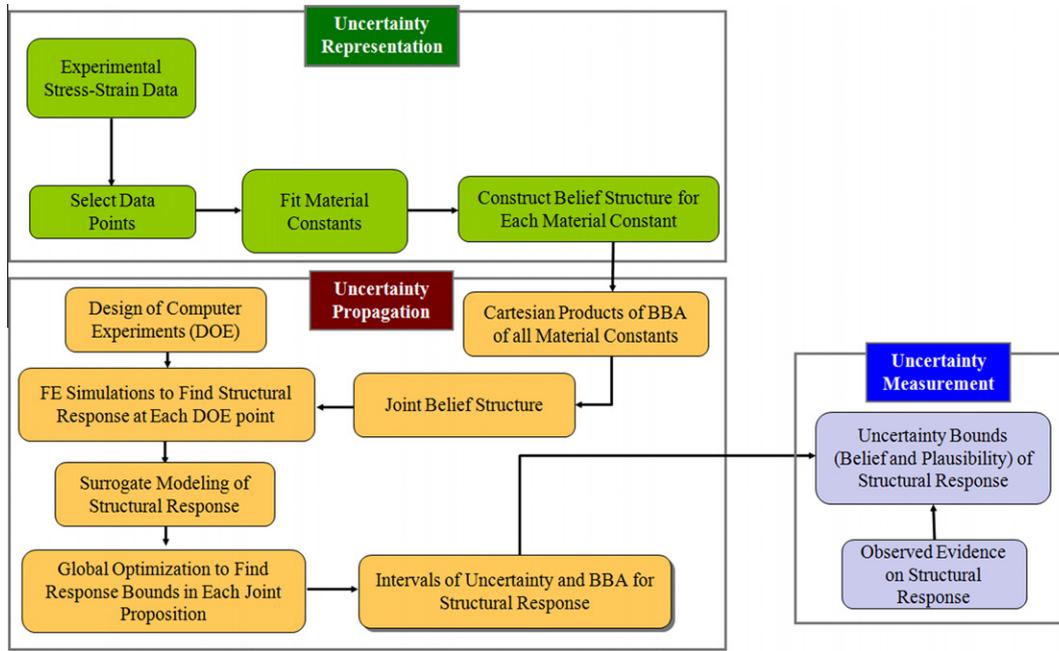
Fig. 4. Three stages of UQ of material models.

representation purpose, the UQ framework uses all possible obtained values of BCJ material constants provided by Table 4 in constructing separate belief structures for material constants. Then, metamodels and global optimization methods is used for propagation of the represented uncertainty through Taylor impact simulations of an AL7075-T651 cylinder using BCJ material model in finite element analysis. Finally, observed evidence on simulation responses are used in determination of target propositions to estimate uncertainty measures. Detailed explanation of UQ procedure with corresponding results is provided here.

6.1. Uncertainty representation

For the purpose of uncertainty representation of BCJ material constants using evidence theory, separate belief structures for each uncertain parameter (six material constants of BCJ flow equation) should be constructed. Here, the derived data for material constants of BCJ plasticity model (see Table 4) reflecting uncertainty in behavior of the 7075-T651 aluminum alloy is used as available evidence in the construction of belief structures. The hardening constants of the model are treated as deterministic since only one data set (see Table 2) is available for their determination.

Salehghaffari and Rais-Rohani [28] developed a general methodology that can extract the necessary information from available data, knowledge, and expert opinions for uncertain parameters and express them in the mathematical framework of evidence theory. The methodology involves two principal steps (1) representation of uncertain parameters in interval form using all available data and expert opinions through drawing bar charts of existing evidence; and (2) categorization of different types of relationship between all adjacent intervals of uncertainty and determination of a suitable belief structure that explains correctly the observed relationship in the context of evidence theory (see Fig. 5 as an example). Based on the developed methodology, two adjacent intervals can be identified as having ignorance, conflict, or agreement relationship. The distinction depends on the number of data points in each interval. For example, the belief structures for ignorance (number of data points in one interval is far greater than those in its adjacent interval) and conflict (number of data points
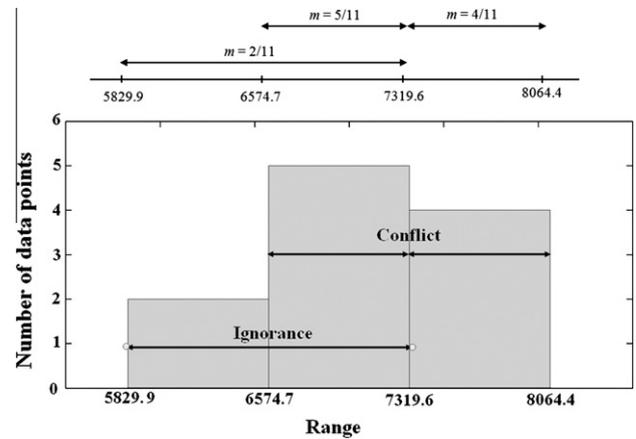

Fig. 5. Data distribution and the corresponding belief structure for constant C_5.

in each interval is large enough to support that interval) relationships take the form of Eqs. (23) and (24), respectively.

$$m(\{I_1\}) = \frac{D_1}{D_1 + D_2} \tag{23a}$$

$$m(\{I_1, I_2\}) = \frac{D_2}{D_1 + D_2} \tag{23b}$$

$$m(\{I_1\}) = \frac{D_1}{D_1 + D_2} \tag{24a}$$

$$m(\{I_2\}) = \frac{D_2}{D_1 + D_2} \tag{24b}$$

where D_1 and D_2 are the number of data points in adjacent intervals I_1 and I_2, respectively. When two adjacent intervals have nearly equal number of data points, they are said to be in agreement and the two intervals are combined into a single one. The BBA expressions in Eqs. (23) and (24) indicate how the degree of belief in

one or more intervals would be calculated. The reader is referred to [28] for further details on representation of uncertain parameters in intervals with assigned BBA.

Following this methodology, a separate belief structure for each uncertain material constant is constructed for 7075-T651 aluminum alloy (see Table 6) using the data provided in Table 3. As an example, the dataset used to construct a belief structure for constant C_5 along with the corresponding belief structure is shown in Fig. 5.

6.2. Uncertainty propagation

A nonlinear finite element analysis (FEA) of Taylor impact test of a 7075-T651 aluminum alloy solid cylinder is used for propagation of the represented uncertainty in Table 6. Simulation responses of large deformation process are affected by all material constants of BCJ plasticity model. To determine the effects of all uncertain material constants, a joint belief structure of their represented uncertainty should be constructed before the uncertainty can be propagated. A joint belief structure is similar in nature to the joint probability density function in probability theory [24,25], and is obtained by Cartesian products of the constructed belief structures of all uncertain parameters [24–27] (see Table 6). This considers all possible combinations of intervals for six material constants of the BCJ flow equation in separate propositions of the joint belief structure. In fact, each joint proposition includes six intervals corresponding to constants C_1–C_6. The BBA of each joint proposition is obtained by multiplication of the final BBA found for each interval of one material constant with those of the other material constants involved in the Cartesian product.

In the context of evidence theory, uncertainty propagation means determination of bounds (intervals) of structural response in each proposition of the joint belief structure. To propagate the represented uncertainties of BCJ constants, final deformed length and radius of the selected cylinder, which are the two main measures of plastic deformation, are considered as structural response.

Unlike the joint probability density function, a joint belief structure cannot be expressed by an explicit function as it includes a number of disjoint propositions, each of which gives one possible combination of intervals for uncertain variables. Propagation of the joint belief structure requires the evaluation of system response for every combination of uncertain parameter values within each joint proposition with the aim of finding the corresponding bounds of the structural response. Performing a nonlinear FEA for every point within each joint proposition is impractical. To reduce the computational cost, we rely on design and analysis of computer experiments and use the following steps for uncertainty propagation as outlined by Fig. 4:

1. Latin hypercube sampling (LHS) technique is adopted to generate 60 separate samples (training points) for material constants C_1–C_6 of BCJ plasticity model. The universal set that spans over the constructed belief structures for all six uncertain material constants of BCJ flow equation as shown in Table 6 are considered in selecting the bounds for generation of the random samples (uncertain material constants).

2. For each training point, we performed FE simulation of Taylor impact test on the cylinder with a 30-mm length and 4.85-mm radius colliding with a velocity of 267 m/s into a rigid plate using an explicit nonlinear FE code LS-DYNA, v 971. The derived hardening constants of BCJ plasticity model (constants C_7–C_{18}) in Table 3 are used in all FE simulations while flow constants (C_1–C_6) are determined by the generated training points.

3. With 60 training points and their responses identified in steps 1 and 2, accurate surrogate models based on Radial Basis Functions (RBFs) are developed to establish an explicit relationship between material constants of BCJ flow equation and the final deformed radius and length. RBF has been used successfully in several investigations for fitting a wide range of response functions with different forms of nonlinearly and dimensionality [29,30]. Since RBF is an interpolation model, ten randomly selected design points (different from any of the training points) within the global bounds of the material constants of BCJ flow equation are used as test points for the evaluation of error statistics to ensure sufficient accuracy of the constructed RBF-based surrogate models.

4. Finally, with each joint proposition providing the bounds or side constraints for material constants of flow equation for BCJ plasticity model, a global optimization (i.e., Genetic Algorithm) technique is applied to the constructed RBF metamodels to find the minimum and maximum values of structural response (radius and length of the deformed cylinder). This procedure is repeated for all the joint propositions of material constants to find the corresponding belief structure for deformed radius and length of cylinder. Hence, the propagated belief structure for structural response is obtained.

6.3. Uncertainty measurement

In the context of evidence theory, uncertainty quantification requires assessment of uncertainty measures (belief, plausibility) for a defined target proposition set using the obtained propagated belief structure. Konokman et al. [31] reported an experimental deformed length of 26.40 mm and radius of 5.76 mm for the cylinder with the same material and geometric properties as those used here for Taylor impact simulations. Here, we define 90% and 95% precision intervals for experimental deformed length and radius of the cylinder and consider them as target proposition set for estimation of uncertainty measures.

To quantify the uncertainty of the BCJ plasticity model, we add BBA of those propagated intervals covered by experimental precision intervals to find belief and add BBA of those intervals intersecting the experimental precision interval to determine plausibility according to Eqs. (21) and (22), respectively. The estimated belief and plausibility for 90% and 95% experimental precision intervals for both deformed radius and length are provided in

Table 6
Belief structures of material constants of BCJ flow equation for 7075-T651 aluminum alloy.

Interval No.	C_1		C_2		C_3	
	Range	BBA	Range	BBA	Range	BBA
1	[262.03,310.17]	5/11	[127.89,187.83]	6/11	[22.30,81.94]	6/11
2	[310.17,358.31]	4/11	[67.95,187.83]	2/11	[22.30,141.57]	2/11
3	[310.17,406.45]	2/11	[187.83,247.77]	3/11	[141.57,201.21]	3/11
	C_4		C_5		C_6	
1	[633.9,890.34]	5/11	[6574.7,7319.6]	5/11	[241.26,291.49]	7/11
2	[375.85,890.34]	2/11	[7319.6,8064.4]	4/11	[155.81,291.49]	4/11
3	[118.6,375.85]	4/11	[5829.9,7319.6]	2/11		

Table 7
Estimated belief and plausibility for experimental precision intervals of deformed length and radius.

Precision (%)	Deformed length (mm)		Deformed radius (mm)	
	Bel	Pl	Bel	Pl
90	0.004	0.928	0.001	0.897
95	0.002	0.899	0.001	0.891

Table 7. As indicated, the estimated values of belief and plausibility for experimental precision intervals of deformed length are slightly higher than those of the deformed radius. Also as expected, for both deformed length and radius, the estimated values of uncertainty measures of 90% precision intervals are higher than those of 95% precision intervals. The gap between belief and plausibility for experimental precision intervals is indicative of epistemic uncertainty embedded in the BCJ plasticity model. The high estimated values of plausibility for precision intervals (target proposition sets) indicate that the presented approach is valid for determination of the BCJ material constants. It also verifies the accuracy of the model to simulate a large deformation process.

7. Conclusions

A physics-guided numerical fitting approach was presented for determination of the material constants of the BCJ plasticity model. The suggested approach relies on the underlying physics at different stages of the fitting process. The approach used experimental data on forward-to-reverse yield of 7075-T651 aluminum alloy to determine the material constants of the hardening equations while considering the Baushinger effects. Four stress–strain curves at different strain rate and temperature ranges were used to derive the material constants of the flow equation. Moreover, an evidential uncertainty quantification method was employed to quantify the uncertainty in the model as well as the presented numerical fitting approach. Different groups of stress–strain curves were used to obtain all possible values of material constants for the flow equation. The data obtained were used to represent existing uncertainty in the material constants that were propagated through FE Taylor impact simulations of 7075-T651 aluminum alloy cylinder. Based on the results of this study, the following conclusions are drawn:

- The proposed fitting method considers the underlying physics in finding the constants of BCJ material model.
- By separating the fitting process into separate stages, the process of fitting the material constants was simplified.
- The predicted stress–strain curves at different temperatures and strain rates showed good agreement with the experimental data.
- The evidential reasoning approach provided the necessary framework for uncertainty quantification of material constants in BCJ material model by considering both aleatory and epistemic uncertainties.

Uncertainty quantification results indicated the validity of the presented numerical fitting approach and the capability of the model to simulate large deformation processes.

Acknowledgments

References

[1] G.R. Johnson, W.H. Cook, Engineering Fracture Mechanics 21 (1985) 31–48.
[2] Y.C. Lin, X.M. Chen, Computational Materials Science 49 (2010) 628–633.
[3] T.J. Holmquist, G.R. Johnson, Journal of Physics IV France 1 (1991) 853–860.
[4] D. Samanataray, S. Mandal, A.K. Bhaduri, Computational Materials Science 47 (2009) 568–576.
[5] T. Shirakashi, K. Maekawa, E. Usui, Bulletin of the Japan Society of Precision Engineering 3 (1983) 161–166.
[6] D.J. Bammann, International Journal of Engineering Science 22 (1984) 1041–1053.
[7] D.J. Bammann, M.L. Chiesa, M.L. Horstemeyer, L.I. Weingarten, Failure in ductile materials using finite element methods, Structural Crashworthiness and Failure, in: T. Wierzbicki, N. Jones (Eds.), Elsevier Applied Science, The Universities Press (Belfast) Ltd., 1993.
[8] D.J. Bammann, M.L. Chiesa, G.C. Johnson, Modeling Large Deformation and Failure in Manufacturing Processes, Theoretical and Applied Mechanics, in: T. Tatsumi, E. Wannabe, T. Kambe, (Eds.), Elsevier Science, 1996, pp. 359–376.
[9] M.F. Horstemeyer, From Atoms to Autos, A New Design Paradigm Using Microstructure-Property Modeling, Part 1: Monotonic Loading Conditions, Sandia National Laboratories, Rep. No. Sand2000-8662, 2001.
[10] E.B. Marin, D.J. Bammann, R.A. Regueiro, G.C. Johnson, On the Formulation, Parameter Identification and Numerical Integration of the EMMI Model: Plasticity and Isotropic Damage. SAN D2006-0200, Sandia National Laboratories, 2006.
[11] G.T. Gray, S.R. Chen, W. Wright, M.F. Lopez, Constitutive Equations for Annealed metals Under Compression at High Strain Rates and High Temperatures, Los-Alamos National Laboratory, LA-12669-MS, 1994.
[12] Y.B. Guo, Q. Wena, M.F. Horstemeyer, International Journal of Mechanical Science 47 (2005) 1423–1441.
[13] B. Coleman, M. Gurtin, Journal of Chemical Physics 47 (1967) 597–613.
[14] J.B. Jordon, M.F. Horstemeyer, K. Solanki, Y. Xue, Mechanics of Materials 39 (2007) 920–931.
[15] Q. Guo-zheng, L. Ke-wei, Z. Jie, C. Bin, Transaction of Nonferrous Metals Society of China 19 (2009) 537–541.
[16] W.S. Lee, W.C. Sue, C.F. Lin, C.J. Wu, Journal of Materials Processing Technology 100 (2000) 116–122.
[17] A.P. Reynolds, S.C. Baxter, Materials Science and Engineering A 285 (2000) 265–279.
[18] A.P. Dempster, Journal of the Royal Statistical Society, Series B 30 (1968) 205–247.
[19] G. Shafer, A Mathematical Theory of Evidence, Princeton University Press, Princeton, NJ, 1976.
[20] D. Dubois, H. Prade, Possibility Theory: An Approach to Computerized Processing of Uncertainty, Plenum Press, New York, 1988.
[21] R.E. Moore, Methods and Applications of Interval Analysis, SIAM, Philadelphia, PA, 1979.
[22] P. Walley, Statistical Reasoning with Imprecise Probabilities, Chapman and Hall, London, 1991.
[23] G.L. Klir, R.M. Smith, Annals of Mathematics and Artificial Intelligence 32 (2001) 5–33.
[24] H. Agarwal, J.E. Renaud, E.L. Preston, D. Padmanabhan, Reliability Engineering & System Safety 85 (2004) 281–294.
[25] H. Bae, R.V. Grandhi, R.A. Canfield, Reliability Engineering & System Safety 86 (2004) 215–225.
[26] H. Bae, R.V. Grandhi, Sensitivity analysis of structural response uncertainty propagation using evidence theory, Structural and Multidisciplinary Optimization 31 (2006) 270–279.
[27] E. Alyanak, R.V. Grandhi, H. Bae, Engineering Optimization 13 (2008) 923–935.
[28] S. Salehghaffari, M. Rais-Rohani, Epistemic uncertainty modeling of Johnson–Cook plasticity model using evidence theory, in: 13th AIAA/ISSMO Multidisciplinary Analysis and Optimization Conference, Fort Worth, Texas, August 9–13, 2010.
[29] S. Salehghaffari, M. Rais-Rohani, Thin-Walled Structurs 49 (2011) 397–408.
[30] H. Fang, M. Rais-Rohani, Z. Liu, M. Horstemeyer, Computers and Structures 83 (2005) 2121–2136.
[31] H.E. Konokman, M. Çoruh, A. Kayran, Acta Mechanica 220 (2011) 61–85.